Materials Challenges for the Fusion Nuclear Science Facility‡

A. F. Rowcliffe, L. M. Garrison*, Y. Yamamoto, L. Tan, Y. Katoh

Oak Ridge National Laboratory, One Bethel Valley Road, Oak Ridge, TN 37831
*Corresponding author, garrisonlm@ornl.gov

Abstract
The phased development and component testing mission of the Fusion Nuclear Science Facility (FNSF) implies a unique scenario for the development of structural and plasma-facing materials. The phased development of the machine and the capability to periodically remove and replace power core sectors allows for the introduction of materials and components with progressively improved operating characteristics throughout the lifetime of the machine. In addition, the machine components removed at each operational phase will provide the first opportunity to test and examine materials irradiated to useful neutron fluences in a fully integrated fusion environment. Options for structural and plasma-facing materials are considered and a preliminary set of materials identified to meet the challenges of power core components and for the machine-lifetime components such as the vacuum vessel and the structural ring. The status of FNSF-relevant materials research and development within the US fusion material program is summarized, and future directions for developing advanced materials to enable the long-term missions of an FNSF are discussed.

1. Introduction

This paper presents a preliminary evaluation of the materials challenges presented by the conceptual design [1] for a Fusion Nuclear Science Facility (FNSF) to bridge the development gap between ITER and a demonstration power plant (DEMO). Here the FNSF specifically denotes the concept that has been studied in the recent Fusion Energy System Studies (FESS) supported by the US Department of Energy, also called the FESS–FNSF, which is examining a conventional aspect ratio tokamak. The FNSF is an experimental machine designed to establish the reliable performance of the critical fusion system technologies required in DEMO and power plants. The FNSF horizontal maintenance system [2] allows for periodic removal, examination, and replacement of full power core sectors.

These activities will provide critical information on material performance in a fully integrated system to complement the single-effects irradiation database on candidate materials generated by any of the proposed accelerator based, intense, 14 MeV neutron sources such as the European proposed DEMO-Oriented Neutron Source (DONES), the Japanese proposed advanced fusion neutron source (A-FNS), or the International Fusion Materials Irradiation Facility (IFMIF) [3]. It is considered essential to have information from both a FNSF facility and

a separate 14MeV neutron facility before proceeding to the final engineering design of a fusion nuclear power plant. Throughout the lifetime of the FNSF, there will be a continuing requirement for access to a fusion-relevant neutron source to validate the performance of the advanced materials required to sustain the increasingly aggressive requirements of the phased development of power core components.

Based on an initially conservative set of operating conditions (operating temperature range, neutron damage, helium generation levels, and mechanical loading) the available materials choices are considered for the removable power core components (first wall (FW), blanket, divertor),the flow channel inserts (insulators) for the dual-coolant lead–lithium (DCLL) blanket, and the machine-lifetime components (vacuum vessel, structural ring, low-temperature magnet shield). Possible options are considered for more advanced materials to meet the requirements of the phased increases in operating temperatures and neutron damage exposure in the progression toward DEMO-like conditions. Recent progress on these FNSF-relevant options is summarized. There are numerous other materials that are essential yet require significant research and development (R&D) to enable engineering design of the FNSF, such as for diagnostic systems, magnets, radio frequency (RF) launchers, heat exchangers, and tritium controls. However, discussion of challenges for these materials is outside the scope of the present article.

2. First wall and divertor materials

2.1 First wall

The FNSF FW concept is a thin tungsten (W) layer coated on a RAFM steel structural material. The purpose of the W layer on the FW is to (1) protect the blanket components from temperature excursions during any transient (edge localized modes, ELMs) and off-normal events (disruptions) in the device and (2) protect the blanket from erosion from ions impacting the wall. A thin W layer is advantageous to maximize the number of neutrons reaching the breeding zone, whereas a thicker W layer has the advantage of further reducing the temperature in the steel components of the FW. Additionally, the thickness of the W layer has to be sufficient to not be eroded during the lifetime of the component. The temperature gradient through the FW layer depends on the thickness of the layer, and thus different thicknesses would have a different stress state. In turn, designs with different temperature profiles could lead to different neutron-irradiated property changes because irradiation defects have temperature dependent formation. The optimal FW layer thickness must be a balance of all these factors. As a starting point of comparing the effects of different FW thicknesses, simulations for the FNSF project have used a 2, 0.5, or 0.2 mm thickness for the W layer.

The steady state heat flux to the FW from plasma radiation is estimated to be approximately 0.25 MW/m^2. In addition to the heat flux from the plasma radiation, there will be a contribution to the heat flux from the flux of ions and neutral atoms incident on the FW. This contribution to the total heat flux on the FW from the particles cannot be neglected and would need to be modeled in more detail during the R&D phase of the FNSF design. Moreover, during plasma startup, power excursions, or other operations the heat flux to the FW will be higher than the steady state value. One of the acceptance criteria for any FW design would be withstanding the necessary steady state and off normal heat flux loads for the desired lifetime of the component without failure.

Table 1 lists some estimated steady state and off-normal temperature and stress values for the FW surface and at the interface with the steel, as calculated by Blanchard et al. using a 0.5 mm thick W layer [4]. The outboard (OB) values were the focus of that study because they are more severe than the inboard (IB) side values. The values summarized in Table 1 are the maximum values for the different modeled scenarios and do not capture the dynamic and spatially varied distribution of those properties after the off-normal events (found in Ref. [4]). The maximum values are of use here for the discussion of conditions the W components must withstand. As noted by Blanchard et al., for the disruption and ELM simulated, the temperatures for the surface of the FW are well below the melting temperature of W, but there would be plastic strain [4]. It is important to consider that temperatures above tungsten's recrystallization temperature (~1200-1500°C depending on the microstructure) may be considered failure because of the negative mechanical property changes in W above recrystallization. More experimental testing would be needed to determine if recrystallization is allowable in the FW and divertor components of the FNSF. At the W-to-steel interface, the temperature rise after a disruption could damage the steel; but during steady state operation and after an ELM, there is no predicted failure [4]. The model used in Ref. [4] uses unirradiated properties of W. Because of the limited neutron irradiation data available, there is a need for experimental material science to develop constituency relationships for properties after neutron irradiation.

Table 1. Estimated heat fluxes and stress levels for first wall and divertor components in the FNSF, compiled from [4], in steady state (SS) and after ELMs and disruptions. Note, the OB FW surface SS heat flux only considers plasma radiation, so the total heat flux would be higher.

	SS heat flux (MW/m^2)	SS max T (°C)	SS stress (MPa)	Max T after ELM (°C)	Max stress after ELM (MPa)	Max T after disruption (°C)	Max stress after disruption (MPa)
OB FW surface	0.25	507	345	739	300	1767	800
OB FW W-steel interface (W side)	—	496	345	536	340	959	546
OB divertor	7.55	1874	484	3200	100	2973	98
IB divertor	2.76	—	—	—	—	—	—

The neutron wall loads (NWL) and estimated displacement per atom (dpa) values for the OB and IB FW are listed in Table 2 for each of the phases of the FNSF program; a prototypical power plant estimate also is listed. For each successive phase of the FNSF, it is assumed that the FW, divertor, and other components inside the vacuum vessel would be replaced; so the dpa would accumulate during one phase before change-out. The dpa will increase as the phases continue because it is planned that the plasma on time, total length of phase, and other details of the plasma operation will increase in each operational phase. The FW and divertor will be rebuilt for each phase, which allows for design or material choice changes and upgrades in later phases; but those details have not been accounted for in the information in Table 2.

The NWL values in Table 2 were calculated by Davis et al. [5]. Their calculation assumed a 2 mm thick W layer on the FW. To estimate the dpa for all the components, first the neutron fluence to the blanket structural material (NWL × years of operation × percentage of

plasma on time) was multiplied by ten to approximate the dpa for a RAFM type steel. Then, to estimate the OB FW W layer dpa, the blanket structural material dpa values were multiplied by a factor of 0.3, which is the relation found by Sawan as the ratio of steel dpa to W DPA for the same incoming magnetic fusion energy spectrum neutron flux [6]. Finally, the dpa estimates for the other W components were scaled based on the ratio of their NWLs and the NWL of the OB FW W. Of course, a more accurate estimate of the dpa in the W components would require a more detailed neutronics model of the full reactor system, but these values in Table 2 represent an order of magnitude indication of goals for designing W materials.

Table 2. Estimated NWLs in (MW/m^2) from Ref. [5] and estimated accumulated dpa for FW and divertor components throughout the FNSF phases and compared with prototypical tokamak power plant values. Phase 1 is non-nuclear and will only use helium (He) and hydrogen (H) plasmas. Phase 2 will move to deuterium-deuterium (DD) fusion plasma but with negligible neutron dose. Phases 3-7 will utilize a deuterium-tritium (DT) fusion plasma.

	FNSF phase	1	2	3	4	5	6	7	Power plant
	Mode	He/H	DD	DT	DT	DT	DT	DT	DT
	Years in phase	1–2	2–3	2.75	4.5	5	6.5	6.5	40
Plasma on time	% per year		15–50	15	25	35	35	35	85
	Days per year		55–183	55	91	128	128	128	310
Component									
OB FW W	NWL	0	0	1.75	1.75	1.75	1.75	1.75	2.25
	dpa	0	0	2	6	10	13	25	47.1–62.8
IB FW W	NWL	0	0	1.31	1.31	1.31	1.31	1.31	1.68
	dpa	0	0	2	5	7	9	19	35.3–47.0
Inner divertor	NWL	0	0	0.79	0.79	0.79	0.79	0.79	1.02
	dpa	0	0	1	3	4	6	11	21.3–28.4
Dome	NWL	0	0	0.66	0.66	0.66	0.66	0.66	0.85
	dpa	0	0	1	2	4	5	10	17.8–23.7
Outer divertor	NWL	0	0	0.76	0.76	0.76	0.76	0.76	0.98
	dpa	0	0	1	3	4	6	11	20.5–27.3
Blanket structural material	NWL	0	0	1.75	1.75	1.75	1.75	1.75	2.25
	dpa	0	0	7	20	31	40	80	150–200
	T max/min (°C)	>400	>400	550/350	550/350	600/400	650/450	650/450	650/450
	Material	Gen1-RAFM	Gen1-RAFM	Gen1-RAFM	Gen1-RAFM	CNA	CNA or ODS	ODS	ODS

ODS = oxide dispersion strengthened; CNA = cast nanostructured alloy

Again, note that the temperature and stress estimates in Table 1 were completed with a model of the FW using a 0.5 mm thick W layer, whereas the model used to calculate the NWL in Table 2 used a 2 mm thick W layer; but together they give an indication of the area in parameter space

that is the goal of the FNSF FW W layer. Comparing the thermomechanical results from Table 1 with the expected dpa to the FW in Table 2, it is clear that the FW structure must withstand these temperature and stress excursions while under moderate to severe amounts of neutron irradiation, ranging from 2 dpa in the first nuclear phase to 25 dpa in the final phase, phase 7, for the OB FW W layer.

The FNSF design has not yet specified the fabrication method to be used for the thin W layer on the steel FW, so several possibilities are discussed here. The eventual selected FW material will have to meet many requirements including, but not limited to, sufficient thermal conductivity, crack resistance, neutron damage resistance, erosion resistance, and limited tritium retention. Because the existing FW technologies are at an early stage of development, it is unclear if the examples mentioned here will meet all the desired requirements, but these examples represent the current state of the art and avenues for potential future development. The testing needed to select the FW material for the first phase of the FNSF is further discussed in Section 2.3.

Existing technologies for coating a thin layer of W on steel—including high-temperature bonding (e.g., forging or hot rolling), plasma-spraying, explosive bonding, and ultrasonic welding—are in various stages of maturity. A high-temperature bonded W-to-steel joint is probably less attractive than other joining options because W and iron form a brittle intermetallic phase when in contact at high temperature. Of course, since the FW will be at elevated temperature during service, it would be possible for such a brittle phase to develop over time, even if it were not present during fabrication, and become a potential point of failure. This behavior needs to be tested with long-term thermal aging and heat flux cycling experiments, which are a common tests needed for any of the technologies discussed below.

A technology that could be explored for fabricating the FNSF FW is plasma-spraying, which could be used to deposit W onto a bulk steel component or even deposit W and steel together to create a functionally graded layer [7]. Generally, a functionally graded layer has lower stresses from thermal expansion mismatch than an abrupt joint between two dissimilar materials, which would be an advantage for the FNSF FW. However, the plasma-sprayed W and steel would have lower thermal conductivity than bulk materials [7], which would also change the temperature profile reported in Table 1. Plasma-sprayed W has a different microstructure and distribution of trapping sites compared with standard powder metallurgical W, which leads to a different amount of deuterium, and presumably tritium, retention [8]. The difference needs to be more fully tested to accurately predict retention and erosion in a plasma-sprayed FW.

Thin W layers have been successfully joined to an F82H steel alloy baseplate by explosive bonding [9]. The nature of explosive bonding causes energy to be deposited in the joint quickly, minimizing the W and iron intermetallic phase at the boundary. Other solid state joining processes, such as friction stir welding and ultrasonic welding, may be explored because they offer advantages similar to those of explosive bonding.

Although the FW W coating is not itself a structural material, because of the thermal gradients, it will be in a state of stress while also at high temperature under neutron irradiation and plasma exposure. To fulfill its purpose, it must remain bonded to the steel substrate and develop no cracks or eroded areas that allow unacceptable temperature excursions in the steel substrate throughout the entire phase. None of the potential coatings has been fully tested under the necessary conditions for even the first nuclear phase, phase 3, of steady state 507°C, 345 MPa, 2 dpa, and deuterium, tritium, and helium bombardment that will accumulate over 2.75

years of operation. In the pre-FNSF R&D phase, candidate W coating technologies for the FW need to undergo testing across all necessary conditions, as described further in Section 2.3.

2.2 Divertor

The FNSF divertor design has a castellated W plate facing the plasma and is cooled by helium jets on the back side. The design has both an armor section of W directly facing the plasma and a structural W section supporting the castellated W plate. Under the FNSF phase strategy, the whole divertor will undergo postmortem analysis at the end of each phase, and a new divertor will be constructed and installed at the start of each phase. This procedure allows lessons learned in earlier phases to influence and improve the design of the divertor for later phases. Within the space constraints, different divertor designs and materials could be used in different phases. Simulations of the FNSF so far have used properties of unirradiated, unalloyed, standard powder metallurgical polycrystalline W (Tables 1 and 2). The divertor components are estimated to receive from ~1 dpa in phase 3, the first nuclear phase, and up to 11 dpa in phase 7. Although the divertor will receive a lower neutron dose than the FW W layer, the dose may impact the divertor more because of the structural function of some of the W in the divertor. Additionally, sections of the divertor will need to withstand higher temperatures and higher stresses during steady state operation than the FW components.

Limited data are available for neutron-irradiated properties of W. Single-crystal W irradiated in the flux trap region of the High Flux Isotope Reactor (HFIR) at Oak Ridge National Laboratory showed a sharp increase in microindentation hardness with increasing dose [10]. However, its ultimate tensile strength at room temperature showed an initial increase (radiation strengthening) at low doses—less than approximately 0.02 dpa—followed by a decrease in ultimate tensile strength at doses higher than approximately 0.02 dpa. The ultimate tensile strength was lower than the unirradiated value at approximately 0.4 dpa and continued to decrease for doses tested [10]. Additionally, after irradiation to less than 1 dpa at 700–800°C, the W had lost all ductility when tensile tested at 500°C, indicating a shift upward of the ductile-to-brittle transition temperature for relatively low-dose irradiation. Because of this property change after irradiation, W that satisfies the conditions modeled in Ref. [4] in the unirradiated state might fail after doses of even 1 dpa, such as those in phase 3. This example uses data for single-crystal W, but even less neutron irradiation data is available on the more advanced W alloys and W composites that may be considered for use in the FNSF. The sensitivity of W thermomechanical properties to neutron irradiation highlights the importance of developing a database of irradiated materials properties for candidate W materials so FNSF components can be designed with confidence.

Another important factor besides dose in determining the irradiated properties of W is the neutron energy spectrum. Although research reactors such as HFIR are often used for materials tests, these fission-based materials test reactors expose materials to significantly more thermal neutrons than are in a typical fusion reactor spectrum. Thus, for W, the higher thermal neutron flux leads to significantly more transmutation to rhenium and osmium in HFIR than would occur in a typical fusion reactor [10, 11]. The additional transmutation products in W irradiated in HFIR contribute significantly to the hardness increase after irradiation [12]. Irradiations done in HFIR, JOYO, and the Japan Materials Testing Reactor (JMTR) research reactors have resulted in different property changes in W for similar doses because of the different amounts of transmutation in the different reactors [13]. For evaluating W properties for fusion applications, it will be key to generate data with a hard neutron spectrum and ideally a 14

MeV neutron source. Tungsten's property changes during neutron irradiation may impact the FW as well as the divertor; but they will most critically impact the divertor, since it has sections of W that are structural rather than only sacrificial armor.

Based on the required stresses at high temperature and high dpa accumulation in later phases (Tables 1 and 2), it is unlikely that standard powder metallurgical W would survive in the later phases of FNSF operation. In fact, no currently existing W material has been demonstrated to resist these estimated conditions. The pathway to the FNSF will need to include significant development of materials that can withstand the divertor conditions of stress, elevated temperatures, neutron dose, and plasma exposure. Several W-based materials that are currently under development and that may provide a pathway to the FNSF divertor are discussed here. There are no known solid solution alloys with W that both improve ductility and meet the neutron activation requirements of fusion reactors, so more emphasis has been placed on developing W-based composites and W with particle additions [14, 15]. A composite material consists of two or more distinct phases on the macroscopic scale, and for W composites in particular two separate strategies of composites are being considered: (1) composites with one phase of W and one phase of a second element or alloy and (2) composites where both phases are W but the phases are distinguished based on their processing route and resulting mechanical properties.

Tungsten-copper laminated composites have been developed that offer superior ductility and fracture toughness to W alone [16, 17]. This type of composite utilizes the ductile copper phase to improve the mechanical properties of the composite as compared to W alone. However, initial irradiation data indicate that these composites lose ductility after low-dose neutron irradiation [18]. Tungsten-copper laminates are intended for a water-cooled divertor system with lower operating temperatures than the FNSF, so are not the ideal option for development for the FNSF. Other W laminates with interlayers other than copper, such as W-steel laminates [19], may be considered for part of the structural region of the FNSF divertor because they could allow for higher operating temperatures than copper while still capturing the benefit of the ductile W foil [20, 21].

An example of an all W composite that relies on different mechanical properties of the two phases of tungsten to give the composite pseudo-ductility is the W-fiber–reinforced, W matrix (W_f/W_m) composite. The W_f/W_m composite utilizes the same motivation as SiC fiber-reinforced SiC composites to make a useful engineering material out of a brittle base material. Variations of W_f/W_m materials have been made via chemical vapor deposition [22, 23] and powder metallurgy [24]. Initial tests of the W_f/W_m composites indicate the fibers provide additional toughness compared with standard W [22].

A group of advanced W alloys and W materials with particle additions, including lanthanum-doped W, potassium-doped W, and ultra-fine-grained W with TiC additions, were irradiated in JMTR and evaluated for microstructural, electrical resistivity, and Vickers hardness changes after irradiation [25]. The study concluded that the second phases in these alloys may slightly reduce irradiation embrittlement by acting as sinks for defects, but none of the alloys emerged as a clear improvement over standard W [25].

2.3 Future R&D needs for FW and divertor materials

Most of the W-based materials proposed for FW or divertor uses are in the early stages of development. Consequently, they often have undergone only one type of testing—for example, heat flux testing or fracture toughness testing, but not both. This makes comparing the different

W-based materials difficult and also makes it impossible to tell at this early stage if any of them will meet all the required properties for the FNSF desired operating conditions. Therefore, for progressing toward an FNSF device, the R&D needs for both the FW and divertor W materials require comprehensive testing of the W materials.

Testing needs for FW and divertor materials:

1. Mechanical properties, including fatigue, creep, tensile, and compression behavior, need to be recorded for any candidate W material both in the unirradiated and neutron-irradiated conditions. Many advanced manufacturing and joining techniques create W microstructures that are dissimilar from standard powder metallurgical W, so each candidate W material needs to be tested to generate reliable data for use in designing the FNSF.
2. Thermal properties, including thermal conductivity after neutron irradiation, response to thermal cycling, and effects of long-term use at elevated temperatures, need to be determined for any candidate W material.
3. Response to neutron irradiation with a 14 MeV neutron source will be important for W because the transmutation cross sections are sensitive to energy, and the transmutation products are known to have a large negative effect on W thermomechanical properties.
4. Response to plasma exposure, including erosion and retention measurements. Any advanced manufacturing technique, particle addition, or composite will change the microstructure of W and create additional internal interfaces that may result in additional trapping sites for tritium. Having data on the candidate W material's interaction with deuterium and tritium is critical so that the tritium inventory can be accurately estimated.
5. Research needs 1–4 could be advanced significantly with single-effects studies. With that starting database, it may be possible to design the first-phase FNSF components with enough confidence to build them. Since it may not be possible to test the full combined effects of neutron flux, particle flux, stress field, and temperature gradient until the operation of the FNSF, the data from the first nuclear phase of FNSF will be critical to inform and improve the design of the FW and divertor for successive phases.

3. Blanket structural materials

3.1 Blanket development conditions for the FNSF mission

The missions and operating metrics for a fusion development pathway from ITER to the fusion power plant described by Ref. [1] define the critical intermediate role of the FNSF in the US program. Of particular relevance to the blanket structural materials are the missions to (1) strongly advance the fusion neutron exposure of all fusion core components toward a power plant level and (2) use and advance power plant-relevant materials in terms of radiation resistance, low activation, operating temperature range, and chemical compatibility. A simplified version of the FNSF phased operations scenario, including the blanket neutron doses and operating temperature requirements for each phase is shown in Table 2. This scenario spans ~23 years of DT operation corresponding to 7.8 full-power-years of neutron exposure at a wall loading of 1.75 MW/m^2.

Beginning with a low-performance DCLL blanket, operating temperatures and neutron dose conditions will be progressively advanced in a series of operational phases leading toward a blanket operating under DEMO-relevant conditions. For each DT phase, it will be possible to replace all the components inside the vacuum vessel, allowing the use of different materials in

different phases. The baseline blanket uses a front-runner Gen1-RAFM alloy, typified by the RCC-MRx code-qualified alloy EUROFER97. It will form the basis of the fabrication and joining technology program to support the pre-FNSF non-nuclear blanket testing program and the construction of the first set of blankets for the power core. EUROFER97 is at a proof-of-principle stage of development at a Technical Readiness Level (TRL) 4 [26, 27].

It is proposed that the initial baseline blanket remain in the machine for the first three phases to enable nuclear break-in while sustaining a peak damage level of ~7 dpa during operation in the 350–550°C temperature range. Current assessments based on fission reactor–based and accelerator-based simulation experiments indicate that radiation-induced property degradation in the Gen1-RAFMs should not significantly impact component performance for neutron exposures below ~20 dpa in the operating range of 350–550°C [28, 29]. There are significant uncertainties involved in this assessment, and it is considered essential to validate the irradiation performance of the Gen1-RAFM by establishing a comprehensive radiation effects database, coupled with predictive modeling of component lifetimes, based on irradiation data from a 14 MeV-peaked neutron source exemplified by DONES/A-FNS/IFMIF. This database should extend over the full range of temperature and neutron dose conditions for phase 3–4 operation. To this end, it is necessary to establish a database of 14 MeV irradiation behavior, from the DONES/A-FNS/IFMIF project or a similar project, well before the beginning of the detailed engineering design phase for FNSF.

Another critical requirement is the development of fusion-relevant design codes. Initial blanket design activities are proceeding utilizing the ITER Structural Design Criteria (ISDC) which are based on ASME code with additional rules for phenomena such as flow localization and creep ratchetting. However, it is generally recognized that the existing codes have only limited value for the FNSF environment and progress towards more detailed engineering design stages will require development of new science-based high temperature design criteria specifically to address the unique requirements of components operating in the fusion environment. Neither the materials properties database nor the current design rules and codes are sufficient to ensure reliable prediction of component performance even for the nuclear break-in operating phases of FNSF. The phased approach to blanket development with incremental increases in neutron exposure and operating temperatures is enabled by a horizontal maintenance system for power core sector removal, examination, and component replacement [2]. A full replacement of both the divertor and blanket components is planned at the end of the first DT phase (7 dpa) to facilitate a full assessment of the mechanical integrity, dimensional stability, corrosion behavior, and other characteristics of the Gen1-RAFM blanket structure.

In addition to the 14 MeV neutron source database, fusion neutron data from phase 3 will be derived from (1) surveillance specimens, irradiated in the FNSF Material Test Module (MTM), that will reflect the influence of the machine operating history and (2) the postmortem examination of power core sectors removed via the horizontal maintenance system. The component data will uniquely incorporate the impact of gradients in nuclear heating, damage rate, and mechanical loading. This combined body of data will form a strong basis for the predictive modeling of component lifetimes for the planned phase 4 operation to a peak dose of 20 dpa on the Gen1-RAFM blanket.

The analysis after phase 3 may indicate that the lifetime performance of the Gen1-RAFM does not meet the requirements for later FNSF phases. To mitigate this risk it will be necessary to initiate full-scale development of higher-performance alloys based on the concept of cast nanostructured alloys (CNAs) early in the pre-FNSF R&D program. Code-qualified alloys with

well-established fabrication technologies for FNSF blanket construction, and proven performance in the 350–600°C range using non-nuclear test stands, are needed as available options for the fabrication of the phases 4–5 blankets. In conjunction with this effort, it will be essential to close the knowledge gap related to the performance of the advanced alloys under fusion-relevant irradiation conditions and to establish a comprehensive irradiation effects database via DONES/A-FNS/IFMIF to support detailed engineering design activities for the phase 4–5 blankets.

To progress toward the development of DEMO-relevant blankets, advanced oxide dispersion strengthened (ODS) alloys will be introduced into the FNSF blanket testing program via test blanket modules (TBMs) during phase 5 operation to demonstrate their capacity to operate at temperatures up to 650°C before full blanket sectors are introduced in phase 6. CNAs are also included as possible options for phase 6, depending on the success of developing the required creep rupture strength and microstructural stability at 650°C under fusion neutron irradiation conditions. A comprehensive irradiation effects database extending to ~65 dpa for the 450–650°C regime will be required via DONES/A-FNS/IFMIF to support the detailed engineering design activities for the CNA- and ODS-based blankets. Both the CNA and ODS classes of alloys are currently at a concept development stage of readiness, TRL 1-3 [26, 27]. Full-scale development programs for the advanced CNA and ODS class of alloys need to be in place at the beginning of the ~20-year FNSF R&D and construction stages. These programs need to be timed to facilitate the insertion of TBMs fabricated with the advanced alloys, beginning in phases 4 and 5 and the deployment of blankets that are capable of operating at temperatures in the 450–650°C regime and sustaining neutron doses of up to 40 dpa and 80 dpa in phases 6–7.

A minimum 20-year timeframe will be required to accommodate the development of the advanced materials to commercialization and code qualification, development of blanket fabrication technologies, evaluation in non-nuclear integrated test programs, and 14 MeV neutron testing in DONES/A-FNS/IFMIF to validate irradiation performance.

3.2 Current status of blanket alloy development

RAFM steels have been developed as candidate structural materials for fusion blanket/FW applications and have demonstrated well-established fabrication capabilities for large-scale industrial heats and flexible components [30]. Studies have shown aggravated effects on the microstructural evolution and subsequent mechanical property degradation of RAFM steels from thermal aging, irradiation, and helium and hydrogen involvement. Thermal aging causes recovery/recrystallization of subgrains, coarsening of $M_{23}C_6$, and the formation of new phases such as Laves and possibly M_6C in the materials. Irradiation results in point defects, dislocation loops, segregation, phase instability, and possible swelling. Helium and hydrogen from neutron reactions and the fusion environment engender the accumulation of bubbles or cavities at boundaries, dislocations, or particle interfaces. These microstructural evolutions tend to exacerbate embrittlement of the materials with increased hardness or strength and decreased impact toughness (i.e., lower impact absorbed energy and higher ductile-brittle transition temperature [DBTT]) [31] . Fig. *1* shows the applicable temperature range of the current RAFM steels, which is confined within a window of ~330–550°C because of the DBTT changes induced by neutron irradiation of Eurofer97 to 16.3 dpa [32] and by thermal aging of F82H for 30,000 and 100,000 h [33].

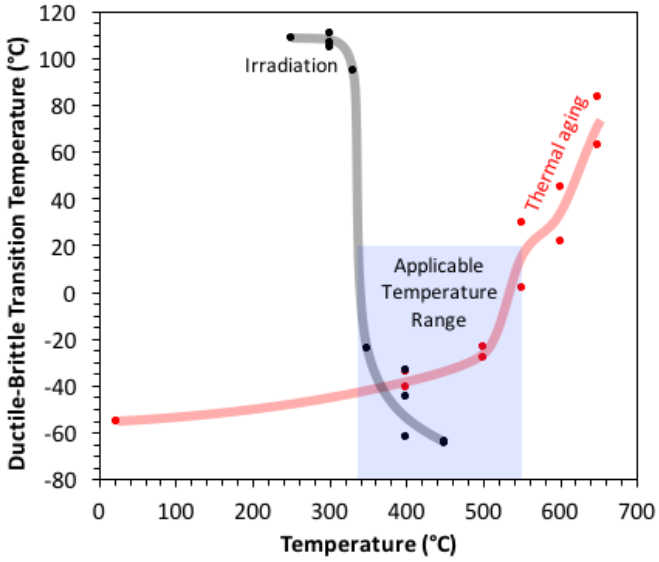

Fig. 1. Effects of irradiation and thermal aging temperatures on the applicable temperature range of the current RAFM steels. Data are adapted from Refs. [32, 33].

Based on materials limitations, the applicable temperature range is likely to be further restricted to an upper bound of ~500°C by other phenomena, such as fatigue/creep–fatigue life interactions and the presence of transmutation-generated helium and hydrogen [34]. A multiphysics modeling approach to optimizing the design and performance of the DCLL FW/blanket system [35] demonstrated the feasibility of maintaining the structure temperature below an upper temperature limit of 550°C through appropriate control of helium flow velocities and operating pressures; adjustments to design configurations and loading conditions to reduce stresses at critical regions and mitigate property limitations were identified.

To develop superior mechanical properties and overcome the narrow applicable temperature range, various approaches have been pursued for RAFM steels, such as thermomechanical treatment and alloy chemistry adjustment assisted by up-to-date computational thermodynamics modeling. Thermomechanical treatment, including nonstandard heat treatments, has been explored to refine microstructures and enhance the density of ultrafine precipitates for improved tensile and creep strength with acceptable ductility and impact toughness [36]. Such optimization attempts, however, are limited by the volume fractions of the dispersed barriers defined by the alloy chemistries of the current RAFM steels.

Second-generation RAFM steels are being developed by optimizing alloy chemistry and by adding new alloying elements to refine microstructures and introduce new strengthening elements. Alloy chemistry optimization has benefited from extensive evaluation of the effects of varying the percentages of common alloying elements such as Ta, W, and Si on mechanical properties of the current RAFM steels (reviewed briefly in Ref. [37]). Zirconium and titanium are primarily considered as new alloying elements because the strict low-activation requirement for shallow land burial of nuclear waste constrains the use and content of many alloying elements [38]. The addition of trace amounts of zirconium (<0.01 wt %) demonstrated some improvements in both impact and creep resistance, despite a negligible influence on yield strength [39]

Recently, CNAs were developed by adding titanium (up to 0.2 wt %) and optimizing the common alloying elements of RAFM steels, which led to a significantly increased amount of MX (M=Ta/Ti/V, X=C/N), about double or more the amount in the current RAFM steels [36].

Compared with Eurofer97 (high angle annular dark-field image in Fig. *2*a adapted from Ref. [40]), the CNA2 (bright-field image in Fig. *2*b [37]) shows significantly larger numbers of ultrafine particles and free dislocations, leading to noticeably increased upper shelf energy of impact toughness, strength, and theoretical sink strength for improved radiation resistance (plotted schematically in Fig. *2*c). The CNAs are expected to have strength and sink strength comparable to that of the lower bound of 9–20 wt % Cr ODS or nanostructured ferritic alloys (NFA) and significantly higher upper shelf energy. The highly dense concentrations of ultrafine particles, primarily in carbides or MC alloys, are believed to be stable dispersed barriers under thermal aging and irradiation conditions [41, 42]; they also exhibited a good helium management capability, based on the examination of helium and Fe^{3+} dual beam irradiated samples [43]. Second-generation RAFM steels such as CNAs are expected to be workable at temperatures above 600°C or even above 650°C, which would satisfy the goals for FNSF operating phase 5 to 6, as listed in Table 2. Currently, composition and processing optimization of CNAs is in progress. Systematic mechanical property tests and irradiation experiments will be pursued to confirm the performance of the alloys. Neutron irradiation experiments, as well as helium- and hydrogen-related properties such as permeation and retention, are planned as critical studies of the new-generation RAFM steels.

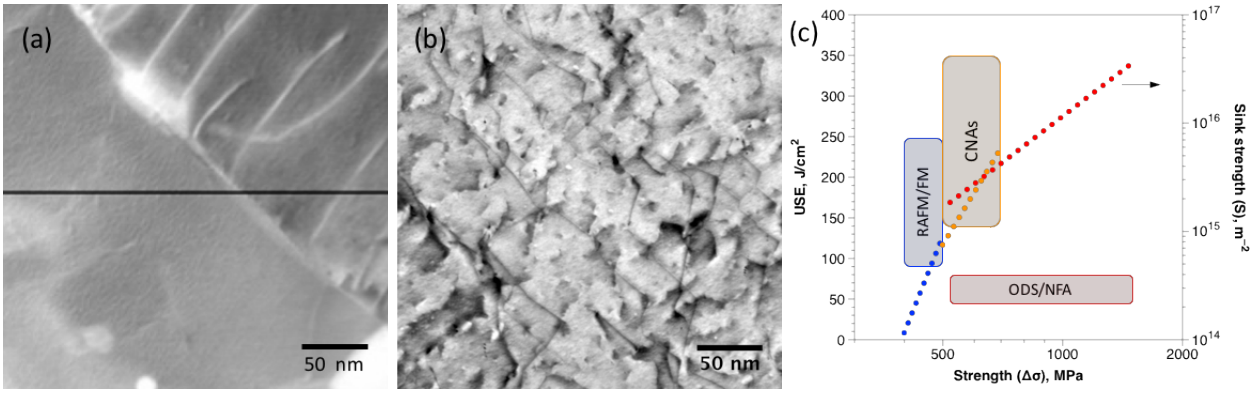

Fig. 2. Comparison of microstructures between (a) Eurofer97 [40]and (b) CNA2 [37], as well as (c) other properties of RAFM/FM, CNAs and ODS/NFA [37].

Iron-based ODS alloys have been developed primarily with 9–20 wt % chromium for fusion applications. Unlike RAFM steels and CNAs manufactured using traditional industrial scale melting techniques, ODS alloys are fabricated by complex mechanical alloying steps, followed by hot consolidation and thermomechanical processing. Mechanical alloying enables the incorporation of a large volume fraction of oxide nanoclusters that are well beyond their solubility in the ferritic matrix. The predominant small oxide nanoclusters (<10 nm in size) in ODS alloys have been reported in a range from ~0.7 vol % in ODS-Eurofer (9Cr: ~5 nm and 1.2×10^{23} m^{-3} [44]) to ~3 vol % in 14YWT (14Cr: ~3 nm and 2×10^{24} m^{-3} [45]). The extremely large number of oxide nanoclusters can effectively pin the submicrometer ferritic grains for superior strength and creep resistance, and help sink/trap irradiation defects and helium atoms for greater radiation resistance and helium management. However, mechanical alloying generally

results in low impact toughness (Figure 2c) with pronounced anisotropic behavior, e.g., significantly lower fracture toughness for the samples in the transverse-longitudinal orientation than in the longitudinal-transverse orientation [46]. The basic microstructure and property comparisons among ODS alloys, CNAs, and current RAFM steels are summarized in Ref. [36]. To obtain greater fracture toughness, advanced 9–10 wt % chromium ODS alloys are being developed via optimized processing conditions in which the matrix undergoes partial phase transformation to strengthen the boundaries [47]. Targeting superior resistance to corrosion and oxidation, novel ODS alloys are being developed based on an Fe-Cr-Al matrix by introducing new oxide components such as ZrO_2 and HfO_2, which have exhibited promising results [43, 48]. A recent review of the developmental status and technical challenges of next-generation RAFM and ODS steels for fusion energy applications can be found in Ref. [49].

4. Flow channel inserts

4.1 Flow channel insert functions and requirements

The flow channel insert (FCI) is one of the key components for blankets using liquid metal as a coolant and/or breeding material, as originally proposed by Malang et al. [50]. The FCI mitigates the magnetohydrodynamic (MHD) pressure drop and enables a higher outlet temperature for the liquid metal than the upper temperature limit for the structural alloy, which makes the DCLL concept attractive for power plants [51]. Two primary functions of the FCI in the DCLL blanket are to electrically insulate Pb-Li from the steel structures and to thermally insulate the steel structures from high-temperature Pb-Li.

Key performance requirements for the FCI material are (1) adequate electrical insulation, (2) adequate thermal insulation, (3) minimized impact on tritium breeding, (4) stability under operating conditions, (5) chemical compatibility with Pb-Li, (6) leak tightness against Pb-Li, (7) ability to withstand mechanical stresses, and (8) retention of all of these qualities throughout its service life. Table 3 lists these requirements and required or preferred attributes for the FCI. The operating environment factors related to items 4 and 8 include developing Pb-LI flow conditions, temperature and field gradients, and repetitive mechanical loading under transient plasma events, in addition to neutron irradiation, elevated temperature, and the chemical environment.

Table 3. Performance requirements for FNSF FCI and status and potentials of primary candidate concepts

	Design requirement	2D SiC/SiC	SiC foam	Metal-encased insulator
Electrical conductivity	<10 S/m inboard, <50 S/m outboard [52]	Need to address effect of transmutations	Need to address effect of transmutations	Bypass conduction is inevitable
Thermal conductivity	<10 W/m·K [52]	Adequate	Adequate	Adequate
Impact on tritium breeding	Minimum	Adequate	Adequate	Not minimum
Stability in operating condition	Up to 80 dpa at 350–800°C	Adequate	Adequate	Need to identify acceptable insulator
Pb-Li compatibility	Up to ~800°C	Need to address effects of flow, electrical current, and transmutations	Need to address effects of flow, electrical current, and transmutations	Unacceptable steel corrosion at >~500°C
Leak tightness	Pb-Li ingress into FCI interior is unacceptable	Need robust hermetic surface	Critical need for robust hermetic casing	Adequate
Mechanical robustness	Withstand external and secondary stress loading	Need to address long-term effect of secondary stress	Need to address cracking issue	Need to address effects and results of steel embrittlement
Potential life-limiting factors		Transmutation effects, environmentally assisted corrosion	Transmutation effects, environmentally assisted corrosion	Radiation stability of insulator, environmentally assisted corrosion

4.2 SiC-based FCI

Silicon carbide (SiC) -based composites, particularly continuous SiC fiber–reinforced SiC-matrix (SiC/SiC) composites, are considered the prime candidates as FCI materials. SiC in a stoichiometric and crystalline form combines intrinsic outstanding advantages, including radiation stability, heat resistance, neutronic transparency, and corrosion resistance against Pb-Li [53-55]. SiC/SiC composites offer additional reliability for structural integrity, crack propagation/opening resistance, and ease of near net-shaping, all beneficial for the FCI application [56]. Moreover, nuclear-grade SiC/SiC composites are industrially available and customizable to desired specifications (Fig. 3).

Fig. 3. Example of fluted core FCI structures made of continuous SiC fiber–reinforced SiC-matrix composites. (Courtesy: Rolls-Royce High Temperature Composites Inc.)

SiC/SiC composites in two-dimensional fabric lay-up architectures are considered to satisfy the general requirements for FCIs in as-manufactured and fission neutron-irradiated conditions [56, 57]. However, a few technical feasibility issues remain to be addressed. They include corrosion behavior under practical conditions involving flowing Pb-Li; impurities, primarily from corroding structural alloys; electrical current flow due to the MHD effect; and solid transmutations in SiC by fusion neutrons [51, 58]. The effects of transmutations on the electrical properties of SiC also need to be clarified [58]. Moreover, the probabilistic matrix cracking and environmentally assisted time-dependent crack opening due primarily to swelling-induced inverse thermal stress must be better understood and minimized through design optimization [59]. An appropriate approach and implementation method to integrate the discrete FCI components into continuous ducts and complex manifold structures remain to be established.

SiC foam-based FCI concepts have been proposed and explored as the alternative to continuous fiber composite concepts [60]. Although a lack of damage tolerance and susceptibility to liquid metal ingress are anticipated and have been proved to be the primary risk factors [61], SiC foams offer the advantages of greater flexibility for enhanced electrical and thermal insulation capability. A potential solution for these critical issues for the open foam–based FCI concept is to adopt continuous fiber composite face plates as the casing material. Most of the critical gap issues for SiC/SiC composites, discussed earlier, are shared with the foams.

4.3 Metal-encased insulator concepts

As a near-term alternative or backup option for SiC-based FCIs, metal-encased insulator structures have been considered. These are often referred to as “sandwich” FCIs because the insulating plate is surrounded by metallic face plates. The European fusion technology program is undertaking the development of such FCIs for its low-temperature starter DEMO blanket [62].

The design space for metal-encased insulator FCIs is bounded by the temperature window for the encasing steel and dose limit for the insulating material. In particular, use of Gen1-RAFM steel limits the operating temperature to below ~500°C because of an unacceptable corrosion rate against Pb-Li. Moreover, alumina may be used only to a dose of a few dpa because of its excessive swelling even at moderate temperatures [63]. To expand the design space, use of alumina-forming corrosion-resistant alloys [64, 65] and more radiation-resistant oxide insulators, such as spinel [66], would be a sensible direction. In addition to the need to expand the design space, challenges for metal-encased insulator FCIs include the fabrication technology. Liquid metal MHD simulations in the FNSF study found that the "sandwich" concept has excessively high pressure drops in the blanket, and would require much lower fusion power (heating) to be feasible [52].

5. Vacuum vessel, structural ring, and low temperature shield

5.1 Material selection

The vacuum vessel is a safety-class component designed to contain tritium and limit public/worker radiation exposure during accident conditions while providing a high-vacuum environment for the lifetime of the plant. The concept for the FNSF vacuum vessel is based on the double-walled ribbed structure adopted by the ARIES-ACT-1 power plant design [67]. Face plates with a 5cm thick section are separated by internal ribs to form channels for helium cooling and to accommodate a W carbide or borated ferritic steel filler material for shielding.

The general requirements for the vacuum vessel structural material are to (1) generate only low-level radioactive waste, (2) generate low levels of decay heat, (3) develop a fracture-resistant microstructure with adequate strength and ductility during fabrication, and (4) maintain mechanical integrity and overall dimensional stability, including void swelling and irradiation creep resistance, during the ~25-year lifetime of the FNSF. Assembly of the vacuum vessel is via on-site welding of segments, and the complexity of the structure raises concerns regarding the viability of carrying out well-controlled post-weld heat treatments (PWHT). The potential for developing high-toughness microstructures during post-welding cooling and eliminating the need for PWHT is therefore a primary attribute needed in the vacuum vessel material. Potential candidate alloys for the vacuum vessel were assessed, including manganese-substituted austenitic stainless steels, RAFMs, low-alloy ferritic steels, and several bainitic steels [68]. It was concluded that the class of reduced-activation 3Cr-3WV bainitic steels [69] possesses the greatest potential to meet the requirements listed above, with the Gen1-RAFMs as a backup. It was shown that meeting the requirements for classification as Class C low-level waste would require the adoption of a set of 17 stringent impurity concentration limits [70] based on the lowest impurity concentrations yet achieved in the large-scale melting and fabrication of a range of reduced-activation and commercial steels.

An operating temperature range of 200–500°C is considered for the vacuum vessel because of competing requirements of tritium control and materials properties. For tritium control, one might assume a higher temperature is better because it prevents the vacuum vessel from being a cold trap, but in fact the more important consideration is that at high temperatures tritium can easily diffuse through the vacuum vessel and become a leakage problem. Thus, a lower temperature may be required to prevent serious tritium leakage. Lower temperatures would also minimize microstructural changes over the ~30 year lifetime of the vessel related to grain boundary segregation, thermally- induced coarsening of the bainitic structure and precipitate structure. On the other hand, maintaining the operating temperature >400°C would

mitigate potential issues related to radiation hardening-induced shifts in DBTT and reductions in fracture toughness. The optimal temperature to satisfy both the tritium control and materials properties is still being evaluated.

The structural ring consists of IB and OB segments bolted to upper and lower blocks to form a closed ring in the poloidal direction and segmented into 16 sectors in the toroidal direction. It is designed to support the vertical loads of the blanket and divertor target plates. It also functions as both a thermal shield and a neutron shield to protect the magnets. The structural ring is in contact with the back of the blanket which is at ~400°C for the nuclear break-in phases and the structural ring is maintained at approximately the same temperature to minimize thermal stresses. This is accomplished either by using the blanket helium cooling system or via separate helium cooling at a low flow rate. There is minimal power deposition in the structural ring and the IB and OB sectors are maintained at the same temperature. The structural material is the Gen-1 RAM plate material fabricated via the same technologies used for the blanket. The introduction of advanced CNAs and ODS alloys in phases 5-7 will enable the FW temperature to increase to ~650°C and would result in an increase in the blanket back wall temperature, and therefore the structural ring temperature, to ~500°C which is still within the allowable operating temperature range for the Gen1 RAFM steel.

The low temperature magnet shield, located immediately outside the vacuum vessel, is also fabricated from the Gen1-RAFM and water cooling is utilized for more effective neutron shielding. The water temperature is maintained below boiling in order to avoid the complications of introducing a pressurized system.

5.2 Radiation damage environment

The sector maintenance system allows for the replacement of the blanket components and divertor before they approach the lifetime dose limits. However, the vacuum vessel and low-temperature shield are regarded as machine lifetime components, with an unknown repair capability. Thus, they must be capable of maintaining structural integrity under the neutron damage levels and transmutation concentrations accumulated during the lifetime of the machine. The structural ring that surrounds and supports the sectors is an intermediate life component, expected to outlive the blankets due to lower dpa/FPY (full power year) and He/FPY. The structural ring would be re-used for some phases, but is expected to be replaced at least once during the life of the FNSF. For a full power fusion plant, the structural ring would likely be replaced more often. An initial estimate of the radiation damage parameters for the long term components, based on a simplified 1-dimensional neutron analysis using the set of FNSF operating parameters shown in Table 4, has been derived [71].

Table 4. FNSF operating parameters

Major radius	4.8 m
Minor radius	1.2 m
Fusion power	526 MW
Peak OB NWL	1.8 MW/m^2
Plant lifetime	30 years
DT operation	23 years
Lifetime neutron exposure	7.8 FPY

Table 5 shows the estimated radiation damage parameters for the structural ring, the vacuum vessel, and low temperature shield. It is assumed that the structural ring would be changed after phase 5, and therefore two sets of damage parameters are shown. The top row values are calculated for the combined phases 3 to 5 (3.3 FPY), and the second row values are for phases 6 to 7 (4.6 FPY). The vacuum vessel and low temperature shield lifetime doses are listed for phases 3 through 7 combined (7.8 FPY). The lifetime exposure of 7.8 FPY for the FNSF is about 5 times lower exposure than expected in a power plant. The calculations include the nuclear heating at the outboard mid-plane, distributions of gamma and neutron spectra, and the radiation damage parameters per FPY—dpa/FPY, He/FPY and H/FPY. In Refs. [71, 72] a safety factor of three is used to estimate the effects of neutron streaming. The damage parameters in Table 5 are the calculated values without the safety factor of three since it is considered essential that engineering solutions will have to be generated to protect against neutron streaming. For both OB and IB side "front" indicates the side of the component closer to the plasma and "back" indicates the side farther from the plasma. The much higher damage parameters on the IB compared to the OB components results from the thicker OB blanket which both reduces the neutron flux and softens the energy spectrum.

Table 5. Radiation damage environment for the structural ring, vacuum vessel, and low temperature shield.

	Component	Lifetime dose (dpa)	Lifetime helium (appm)	Lifetime hydrogen (appm)	Helium/dpa ratio
OB [71]	Structural ring front	0.23 0.32	0.021 0.029	0.10 0.14	0.090
	Structural ring back	0.041 0.057	0.0017 0.0023	0.0080 0.011	0.041
	Vacuum vessel front	0.083	0.0030	0.014	0.036
	Vacuum vessel back	0.042	0.0012	0.0063	0.030
	Low temperature shield front	0.041	0.0012	0.0057	0.029
	Low temp. shield back	0.00063	0.00013	0.00058	0.20
IB [72]	Structural ring front	6.3 8.8	3.3 4.6	16 22	0.52
	Structural ring back	0.57 0.80	0.21 0.29	1.0 1.4	0.37
	Vacuum vessel front	1.0	0.47	2.1	0.45
	Vacuum vessel back	0.18	0.081	0.39	0.46
	Low temperature shield front	0.12	0.065	0.29	0.53
	Low temp. shield back	0.0011	0.0044	0.020	3.9

Tables 2 and 5 illustrate the strong gradients in displacement damage and helium generation rates that occur radially from the blanket FW out to the low temperature shield. Damage rates vary with ~2×10^{-6} dpa/s at the FW, ~7×10^{-8} dpa/s at the front of the structural ring, ~2×10^{-10} dpa/s at the back of the vacuum vessel, and ~1×10^{-12} dpa/s at the back of the low temperature shield. Although the displacement damage and helium concentrations accumulated by the structural ring, vacuum vessel, and low temperature shield (Table 5) are generally considered to be very low, they are not insignificant. For example, although the low temperature shield accumulates a maximum dose of only 0.12 dpa, neutron irradiation data at 50-160°C for ferritic/martensitic steels indicates that these irradiation conditions would be sufficient to increase the yield stress by ~200 MPa [73]. There are no neutron irradiation data available at 400-450°C for the 3Cr-3WV bainitic steel used for the vacuum vessel. However, neutron irradiation data indicates that the radiation hardening of the bainitic steel irradiated in the 50-160°C range is very similar to that of the ferritic/martensitic steels up to 1.2 dpa [73]. If this similarity in behavior of the two steels persists at 400°C then a radiation hardening of ~50 MPa at ~1 dpa would be a reasonable estimate for the lifetime radiation hardening for the vacuum vessel.

Future irradiation programs in support of an FNSF will need to address the low damage and low damage rate environments typical of the structural ring, vacuum vessel, and low temperature shield. The synergistic effects of neutron fluence, flux, and spectrum, irradiation temperature, and the chemical composition and microstructure of the steels must be understood to enable the development of predictive lifetime models for these components.

5.3 Current status of bainitic steel R&D

Bainitic steels containing 2.25 to 3 wt % chromium are attractive structural materials for lifetime component applications in a fusion power system because they have good high-temperature structural properties, can be constructed into complicated components with welding, and potentially have a low capital cost. Under the current FNSF design considerations, of particular interest is the 3Cr-3W-0.2V-0.1Ta-Mn-Si-C containing bainitic steel for construction of the vacuum vessel and the structural ring. The 3Cr-3WV base bainitic steel was reported to exhibit tensile strengths superior to those of high-chromium RAFM steels, such as 9Cr-2WVTa steel, from room temperature to 550–600°C [69]. It also showed a lower DBTT than the RAFM steels at tempered conditions, and the DBTT was as low as −40°C even without tempering [69]. The creep properties of the 3Cr-3WV steels exceeded those of commercially available T22 (2.25Cr-1Mo), T23 (2.25Cr-1.6WVNb), and T91 (9Cr-1MoVNb) steels at 600°C, and the addition of 0.1Ta (to form so-called 3Cr-3WVTa steel) resulted in further improvement in the creep-rupture properties in the temperature range from 550 to 650°C [74, 75]. It was also reported that 3Cr-3WV base bainitic steel weldments with a proper filler wire had sufficient room-temperature impact toughness in the as-welded condition, indicating potentially no requirement for PWHT [76]. In addition, it is a cost-effective material because it contains relatively low amounts of alloying elements. Because of all these features, 3Cr-3WV base bainitic steels are suitable for the production of large volume components, such as the vacuum vessel and the structural ring, for operation conditions not exceeding ~600°C.

The high-temperature mechanical properties of the bainitic steels rely on the formation of carbide-free acicular bainite ferrite and second-phase precipitate strengthening [77]. Since these factors are sensitive to alloying elements, further optimization of the mechanical properties has been attempted with the guidance of computational thermodynamics [78]. It is expected to result in potentially positive impacts on the design availability and the safety margin of structural components in fusion reactor structural applications. Two different alloy design strategies were proposed: (1) improve creep properties of the base material by increasing the amounts of strengthening M(C,N) and (2) decrease cross-weld property inhomogeneity by decreasing the as-normalized (as-cast) hardness. The first task was successfully achieved by modifying the alloy composition of the 3Cr-3WVTa steel with relatively high manganese and nitrogen additions ("Mn-N modified") as shown in Fig. 4. However, the modification also increased the hardness of the as-normalized (as-solidified) material significantly, resulting in an increase in the cross-weld hardness inhomogeneity compared with the original 3Cr-3WVTa steel, as shown in Fig. 5. The Vickers hardness distribution maps of the as-welded materials indicated that both the weld metal and the adjacent heat-affected zone exhibited increased hardness compared with the tempered base metal regions for the original and the Mn-N modified steels (Figs. 5b and 5c, respectively), and the Mn-N modified steel showed much higher hardness than the original steel. This could lead to inhomogeneous stress segregation, which might cause premature failures such as Type IV cracking or stress-induced corrosion cracking. To solve this issue, a second alloy design strategy was applied that combined high additions of manganese with intentionally lowered amounts of

carbon ("Mn-C modified"). The low amount of carbon successfully reduced the hardness of entire cross-weld regions, with a lower increase in the hardness at the weld metal and heat-affected zone, as shown in Fig. 5d. The alloy composition of the Mn-C modified steel was selected to maintain the high hardenability obtained by adding a large amount of manganese to form acicular bainite ferrite, which successfully preserved tensile strengths superior to those of high-chromium ferritic-martensitic steels at temperatures up to 600°C. Preliminary creep property evaluation of the base metal indicated that the minimum creep rates at 550°C were equivalent to those of the original 3Cr-3WVTa steels.

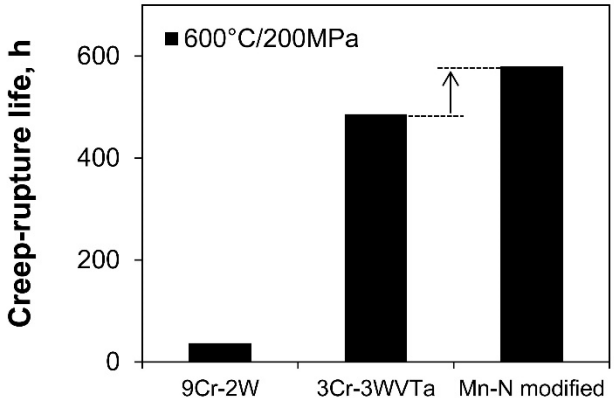

Fig. 4. Creep-rupture life of the original 3Cr-3WVTa and the Mn-N modified bainitic steels tested at 600°C and 200MPa, compared with the life of 9Cr-2W ferritic-martensitic steel.

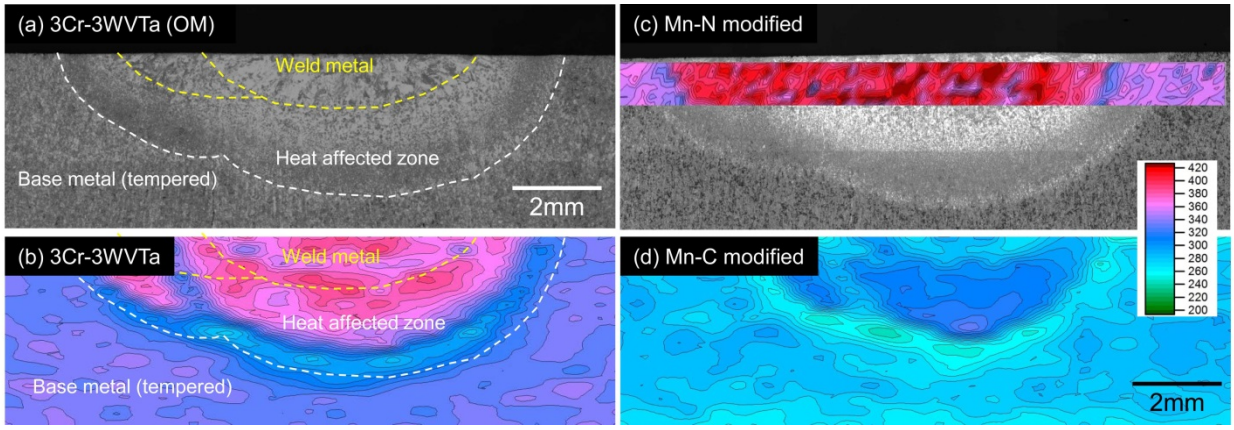

Fig. 5. (a) Cross-sectional micrograph of bead-on-plate gas-tungsten arc welded 3Cr-3WVTa bainitic steel and Vickers hardness distribution maps of (b) the original 3Cr-3WVTa, (c) the Mn-N modified, and (d) the Mn-C modified steels applying the same weld procedure. No PWHT was applied.

5.4 Future directions of bainitic steel R&D

The results of these initial studies suggest that further improvement of balanced properties (i.e. tensile, creep, and cross-weld properties) could be achieved by further extension of computational thermodynamic alloy design strategies. The scale-up effort for Mn-C modified steel is currently in progress, and a comprehensive property evaluation is planned.

6. Conclusions

An initial set of structural and plasma-facing materials has been identified which provide a basis for the continued optimization of conceptual designs for an FNSF power core system and lifetime components. In conjunction with the continued development of radiation damage–resistant materials, data from the post -irradiation examination of components from the first nuclear phase of FNSF will be critical to inform and improve the design of power core components for the successive operational phases.

Two overarching issues impact the timing of a detailed engineering design phase for an FNSF: (1) The earliest possible access to an intense 14 MeV neutron irradiation facility, such as DONES/A-FNS/IFMIF, is essential to validate materials performance for the nuclear break-in phase of operations and for successive phases involving increasingly higher neutron doses, particle fluxes, and operational temperatures. (2) The successful deployment of materials with microstructures engineered for specific mechanical properties and radiation damage resistance depends on the demonstration of advanced fabrication technologies, tailored for the specific requirements of each component, which generate the required start-of life microstructures.

Acknowledgments
This research was supported by the US Department of Energy, Office of Science, Fusion Energy Sciences. This manuscript has been authored by UT-Battelle, LLC, under Contract No. DE-AC05-00OR22725 with the US Department of Energy. The authors wish to acknowledge C. Kessel and the members of the FNSF design team for enlightening discussions on materials issues for the FNSF.

References

[1] C.E. Kessel, FESS team, Overview of the Fusion Nuclear Science Facility (FNSF), a credible break-in step on the path to fusion electricity production, submitted to Fusion Engineering and Design (2017).
[2] L.M. Waganer, Examination of the FNSF maintenance approach, submitted to Fusion Engineering and Design, (2017).
[3] J. Knaster, IFMIF, the European-Japanese efforts under the Broader Approach Agreement towards a Li(d,xn) neutron source, current status and future options. Presented at ICFRM-17, October, 2015
[4] J.P. Blanchard, C. Martin, W. Liu, Effect of ELMs and disruptions on FNSF plasma-facing components, Fusion Eng. Des. (special FNSF issue) (2017).
[5] A. Davis, L. El-Guebaly, P. Wilson, E. Marriott, F.-F. team, Neutronics aspects of the FESS-FNSF, Fusion Eng. Des. (special FNSF issue) (2017).
[6] M.E. Sawan, Damage parameters of structural materials in fusion environment compared to fission reactor irradiation, Fusion Eng. Des. 87(5-6) (2012) 551-555.
[7] J. Matějíček, H. Boldyryeva, Processing and temperature-dependent properties of plasma-sprayed tungsten–stainless steel composites, Phys. Scripta T138 (2009) 014041.
[8] V.K. Alimov, H. Nakamura, B. Tyburska-Püschel, O.V. Ogorodnikova, J. Roth, K. Isobe, T. Yamanishi, Deuterium retention in plasma spray tungsten coatings exposed to low-energy, high flux D plasma, J. Nucl. Mater. 414(3) (2011) 479-484.

[9] D. Mori, R. Kasada, S. Konishi, Y. Morizono, K. Hokamoto, Underwater explosive welding of tungsten to reduced-activation ferritic steel F82H, Fusion Eng. Des. 89(7-8) (2014) 1086-1090.
[10] Y. Katoh, D. Clark, Y. Ueda, Y. Hatano, M. Yoda, A.S. Sabau, T. Yokomine, L.M. Garrison, W. Geringer, A. Hasegawa, T. Hino, M. Shimada, D. Buchenauer, Y. Oya, T. Muroga, Progress in the US/Japan PHENIX project for the technological assessment of plasma facing components for DEMO reactors, submitted to Fusion Science and Technology (2016).
[11] M. Sawan, Transmutation of tungsten in fusion and fission nuclear environments, Fusion Sci. Technol. 66 (2014) 272-277.
[12] X. Hu, T. Koyanagi, M. Fukuda, N.A.P.K. Kumar, L.L. Snead, B.D. Wirth, Y. Katoh, Irradiation hardening of pure tungsten exposed to neutron irradiation, J. Nucl. Mater. 480 (2016) 235-243.
[13] M. Fukuda, N.A.P. Kiran Kumar, T. Koyanagi, L.M. Garrison, L.L. Snead, Y. Katoh, A. Hasegawa, Neutron energy spectrum influence on irradiation hardening and microstructural development of tungsten, J. Nucl. Mater. 479 (2016) 249-254.
[14] S. Wurster, N. Baluc, M. Battabyal, T. Crosby, J. Du, C. García-Rosales, A. Hasegawa, A. Hoffmann, A. Kimura, H. Kurishita, R.J. Kurtz, H. Li, S. Noh, J. Reiser, J. Riesch, M. Rieth, W. Setyawan, M. Walter, J.H. You, R. Pippan, Recent progress in R&D on tungsten alloys for divertor structural and plasma facing materials, J. Nucl. Mater. 442(1-3) (2013) S181-S189.
[15] M. Rieth, S.L. Dudarev, S.M. Gonzalez de Vicente, J. Aktaa, T. Ahlgren, S. Antusch, D.E.J. Armstrong, M. Balden, N. Baluc, M.F. Barthe, W.W. Basuki, M. Battabyal, C.S. Becquart, D. Blagoeva, H. Boldyryeva, J. Brinkmann, M. Celino, L. Ciupinski, J.B. Correia, A. De Backer, C. Domain, E. Gaganidze, C. García-Rosales, J. Gibson, M.R. Gilbert, S. Giusepponi, B. Gludovatz, H. Greuner, K. Heinola, T. Höschen, A. Hoffmann, N. Holstein, F. Koch, W. Krauss, H. Li, S. Lindig, J. Linke, C. Linsmeier, P. López-Ruiz, H. Maier, J. Matejicek, T.P. Mishra, M. Muhammed, A. Muñoz, M. Muzyk, K. Nordlund, D. Nguyen-Manh, J. Opschoor, N. Ordás, T. Palacios, G. Pintsuk, R. Pippan, J. Reiser, J. Riesch, S.G. Roberts, L. Romaner, M. Rosiński, M. Sanchez, W. Schulmeyer, H. Traxler, A. Ureña, J.G. van der Laan, L. Veleva, S. Wahlberg, M. Walter, T. Weber, T. Weitkamp, S. Wurster, M.A. Yar, J.H. You, A. Zivelonghi, Recent progress in research on tungsten materials for nuclear fusion applications in Europe, J. Nucl. Mater. 432(1-3) (2013) 482-500.
[16] J. Reiser, M. Rieth, B. Dafferner, A. Hoffmann, Tungsten foil laminate for structural divertor applications—Basics and outlook, J. Nucl. Mater. 423 (2012) 1-8.
[17] J. Reiser, M. Rieth, A. Moeslang, B. Dafferner, A. Hoffmann, X. Yi, D.E.J. Armstrong, Tungsten foil laminate for structural divertor applications—Tensile test properties of tungsten foil, J. Nucl. Mater. 434 (2013) 357-366.
[18] L.M. Garrison, Y. Katoh, L.L. Snead, T.S. Byun, J. Reiser, M. Rieth, Irradiation effects in tungsten-copper laminate composite, J. Nucl. Mater. 481 (2016) 134-146.
[19] L.M. Garrison, E.K. Ohriner, Fabrication of functionally graded, tungsten steel laminate, DOE-ER-0313/57, (2014).
[20] J. Reiser, M. Rieth, B. Dafferner, A. Hoffmann, X. Yi, D. Armstrong, Tungsten foil laminate for structural divertor applications—Analysis and characterisation of tungsten foil, J. Nucl. Mater. 424 (2012) 197-203.
[21] J. Reiser, S. Wurster, J. Hoffmann, S. Bonk, C. Bonnekoh, D. Kiener, R. Pippan, A. Hoffmann, M. Rieth, Ductilisation of tungsten (W) through cold-rolling: R-curve behaviour, Int. J. Refract. Met. Hard Mater. 58 (2016) 22-33.

[22] J. Riesch, T. Höschen, C. Linsmeier, S. Wurster, J.H. You, Enhanced toughness and stable crack propagation in a novel tungsten fibre-reinforced tungsten composite produced by chemical vapour infiltration, Phys. Scripta T159 (2014) 014031.
[23] J. Riesch, Y. Han, J. Almanstötter, J.W. Coenen, T. Höschen, B. Jasper, P. Zhao, C. Linsmeier, R. Neu, Development of tungsten fibre-reinforced tungsten composites towards their use in DEMO—potassium doped tungsten wire, Phys. Scripta T167 (2016) 014006.
[24] J.W. Coenen, Y. Mao, J. Almanstötter, A. Calvo, S. Sistla, H. Gietl, B. Jasper, J. Riesch, M. Rieth, G. Pintsuk, F. Klein, A. Litnovsky, A.V. Mueller, T. Wegener, J.H. You, C. Broeckmann, C. Garcia-Rosales, R. Neu, C. Linsmeier, Advanced materials for a damage resilient divertor concept for DEMO: Powder-metallurgical tungsten-fibre reinforced tungsten, Fusion Eng. Des. (2016).
[25] M. Fukuda, A. Hasegawa, T. Tanno, S. Nogami, H. Kurishita, Property change of advanced tungsten alloys due to neutron irradiation, J. Nucl. Mater. 442(1-3) (2013) S273-S276.
[26] M.S. Tillack, H. Tanegawa, S. Zinkle, A. Kimura, R. Shinavski, M. Rieth, E. Diegele, L.L. Snead, Technology readiness applied to materials for fusion applications. Presented at ICFRM, October 16-21, 2011
[27] M.S. Tillack, A.D. Turnbull, L.M. Waganer, S. Malang, D. Steiner, J.P. Sharpe, L.C. Cadwallader, L. El-Guebaly, A.R. Raffray, F. Najmabadi, R.J. Peipert, Jr., T.L. Weaver, the ARIES Team, An evaluation of fusion energy R&D gaps using technology readiness levels, Fusion Sci. Technol. 56 (2009) 949-956.
[28] A. Zinkle, H. Muroga, S.J. Möslang, T. Tanigawa, Multimodal options for materials research to advance the basis for fusion energy in the ITER era, Nucl. Fus 53 (2013) 104024.
[29] D. Stork, Developing structural, high heat flux and plasma facing materials for a near-term DEMO fusion power plant: the EU assessment, J. Nucl. Mater 455 (2014) 277-291.
[30] M. Zmitko, N. Thomas, A. LiPuma, L. Forest, L. Cogneau, J. Rey, H. Neuberger, Y. Poitevin, The European ITER test blanket modules: Progress in development of fabrication technologies towards standardization, Fusion Eng. Des. 109 (2016) 1687-1691.
[31] S.J. Zinkle, A. Moslang, Evaluation of irradiation facility options for fusion materials research and development, Fusion Eng. Des. 88(6-8) (2013) 472-482.
[32] E. Gaganidze, J. Aktaa, Assessment of neutron irradiation effects on RAFM steels, Fusion Eng. Des. 88(3) (2013) 118-128.
[33] K. Shiba, H. Tanigawa, T. Hirose, H. Sakasegawa, S. Jitsukawa, Long-term properties of reduced activation ferritic/martensitic steels for fusion reactor blanket system, Fusion Eng. Des. 86(12) (2011) 2895-2899.
[34] R. Lindau, A. Moslang, D. Preininger, M. Rieth, H.D. Rohrig, Influence of helium on impact properties of reduced-activation ferritic martensitic Cr-steels, J. Nucl. Mater. 271 (1999) 450-454.
[35] Y. Huang, Multiphysics modeling of the FW/blanket of the Nuclear Science Facility (FNSF), submitted to Fusion Engineering and Design (2017).
[36] L. Tan, Y. Katoh, A.A.F. Tavassoli, J. Henry, M. Rieth, H. Sakasegawa, H. Tanigawa, Q. Huang, Recent status and improvement of reduced-activation ferritic-martensitic steels for high-temperature service, J. Nucl. Mater. 479 (2016) 515-523.
[37] L. Tan, L.L. Snead, Y. Katoh, Development of new generation reduced activation ferritic-martensitic steels for advanced fusion reactors, J. Nucl. Mater. 478 (2016) 42-49.

[38] H. Tanigawa, Y. Someya, H. Sakasegawa, T. Hirose, K. Ochiai, Radiological assessment of the limits and potential of reduced activation ferritic/martensitic steels, Fusion Eng. Des. 89(7-8) (2014) 1573-1578.
[39] Y.B. Chun, S. Kang, T.K. Noh, D.W. Kim, S. Lee, Y.H. Cho, Y.B. Jeong, Effects of alloying elements and heat treatments on mechanical properties of Korean reduced-activation ferritic-martensitic steel, J. Nucl. Mater, 455 (2014) 212-216.
[40] M. Klimenkov, R. Lindau, E. Materna-Morris, A. Moslang, TEM characterization of precipitates in EUROFER 97, Progress in Nuclear Energy 57 (2012) 8-13.
[41] L. Tan, T.S. Byun, Y. Katoh, L.L. Snead, Stability of MX-type strengthening nanoprecipitates in ferritic steels under thermal aging, stress and ion irradiation, Acta Materialia 71 (2014) 11-19.
[42] L. Tan, Y. Katoh, L.L. Snead, Stability of the strengthening nanoprecipitates in reduced activation ferritic steels under Fe2+ ion irradiation, J. Nucl. Mater. 445(1-3) (2014) 104-110.
[43] C.M. Parish, K.A. Unocic, L. Tan, S.J. Zinkle, S. Kondo, L.L. Snead, D.T. Hoelzer, Y. Katoh, Helium sequestration at nanoparticle-matrix interfaces in helium plus heavy ion irradiated nanostructured ferritic alloys, J. Nucl. Mater. 483 (2017) 21-34.
[44] C. Heintze, F. Bergner, A. Ulbricht, M. Hernandez-Mayoral, U. Keiderling, R. Lindau, T. Weissgarber, Microstructure of oxide dispersion strengthened Eurofer and iron-chromium alloys investigated by means of small-angle neutron scattering and transmission electron microscopy, J. Nucl. Mater. 416(1-2) (2011) 35-39.
[45] A. Hirata, T. Fujita, C.T. Liu, M.W. Chen, Characterization of oxide nanoprecipitates in an oxide dispersion strengthened 14YWT steel using aberration-corrected STEM, Acta Mater 60 (2010) 5686-6596.
[46] T.S. Byun, D.T. Hoelzer, J.H. Kim, S.A. Maloy, A comparative assessment of the fracture toughness behavior of ferritic-martensitic steels and nanostructured ferritic alloys, J. Nucl. Mater. 484 (2017) 157-167.
[47] T.S. Byun, J.H. Yoon, D.T. Hoelzer, Y.B. Lee, S.H. Kang, S.A. Maloy, Process development of 9Cr nanostructured ferritic alloy (NFA) with high fracture toughness, J. Nucl. Mater 449 (2014) 290-299.
[48] K.A. Unocic, D.T. Hoelzer, Evaluation of Pb-17Li compatibility of ODS Fe-12Cr-5Al alloys, J. Nucl. Mater. 479 (2016) 357-364.
[49] S.J. Zinkle, J.-L. Boutard, D.T. Hoelzer, A. Kimura, R. Lindau, G. Odette, M. Rieth, L. Tan, H. Tanigawa, Development of next generation tempered and ODS reduced activation ferritic/martensitic steels for fusion energy applications, accepted to Nuclear Fusion (2017).
[50] S. Malang, V. Casal, K. Arheidt, U. Fischer, W. Link, K. Rust, Liquid metal cooled blanket concept for NET, Pergamon, Oxford, UK, Avingnon, France, 1986, pp. 1273-1280.
[51] N.B. Morley, Y. Katoh, S. Malang, B.A. Pint, A.R. Raffray, S. Sharafat, S. Smolentsev, G.E. Youngblood, Recent US research and development for the dual coolant blanket concept, Fusion Eng. Des. 83 (2008) 920-927.
[52] S. Smolentsev, T. Rhodes, G. Pulugundla, C. Courtessole, M. Abdou, S. Malang, M. Tillack, C. Kessel, MHD Thermohydraulic analysis and supporting R&D for DCLL blanket in FNSF, submitted to Fusion Engineering and Design (2017).
[53] Y. Katoh, L.L. Snead, I. Szlufarska, W.J. Weber, Radiation effects in SiC for nuclear structural applications, Current Opinion in Solid State & Materials Science 16(3) (2012) 143-152.

[54] L.L. Snead, T. Nozawa, Y. Katoh, T.S. Byun, S. Kondo, D.A. Petti, Handbook of SiC properties for fuel performance modeling, J. Nucl. Mater. 371(1-3) (2007) 329-377.
[55] B.A. Pint, J.L. Moser, P.F. Tortorelli, Investigation of Pb-Li compatibility issues for the dual coolant blanket concept, J. Nucl. Mater. 367-370(SPEC. ISS.) (2007) 1150-1154.
[56] Y. Katoh, K. Ozawa, C. Shih, T. Nozawa, R.J. Shinavski, A. Hasegawa, L.L. Snead, Continuous SiC fiber, CVI SiC matrix composites for nuclear applications: Properties and irradiation effects, J. Nucl. Mater. 448(1-3) (2014) 448-476.
[57] Y. Katoh, S. Kondo, L.L. Snead, DC electrical conductivity of silicon carbide ceramics and composites for flow channel insert applications, J. Nucl. Mater. 386(C) (2009) 639-642.
[58] M. Sawan, Y. Katoh, L.L. Snead, Transmutation of silicon carbide in fusion nuclear environment, J. Nucl. Mater. 442(1) (2013) S370-S375.
[59] G. Singh, K.A. Terrani, Y. Katoh, 3D thermo-mechanical assessment of SiC/SiC composite cladding for LWR application, under review for Journal of Nuclear Materials (2017).
[60] S. Sharafat, A. Aoyama, N. Morley, S. Smolentsev, Y. Katoh, B. Williams, N. Ghoniem, Development status of a SiC-foam based flow channel insert for a U.S.-ITER DCLL TBM, Fusion Sci. Technol. 56(2) (2009) 883-891.
[61] S. Smolentsev, C. Courtessole, M. Abdou, S. Sharafat, S. Sahu, T. Sketchley, Numerical modeling of first experiments on PbLi MHD flows in a rectangular duct with foam-based SiC flow channel insert, Fusion Eng. Des. 108 (2016) 7-20.
[62] P. Norajitra, W.W. Basuki, M. Gonzalez, D. Rapisarda, M. Rohde, L. Spatafora, Development of sandwich flow channel inserts for an EU DEMO dual coolant blanket concept, Fusion Sci. Technol. 68(3) (2015).
[63] T. Yano, K. Ichikawa, M. Akiyoshi, Y. Tachi, Neutron irradiation damage in aluminum oxide and nitride ceramics up to a fluence of 4.2 10 26 n/m 2 J. Nucl. Mater. 283-287(Part 2) (2000) 947-951.
[64] B.A. Pint, J.L. Moser, P.F. Tortorelli, Liquid metal compatibility issues for test blanket modules, Fusion Eng. Des. 81(8-14) (2006) 901-908.
[65] Y. Yamamoto, B.A. Pint, K.A. Terrani, K.G. Field, Y. Yang, L.L. Snead, Development and property evaluation of nuclear grade wrought FeCrAl fuel cladding for light water reactors, J. Nucl. Mater. 467 (2015) 703-716.
[66] C. Kinoshita, S.J. Zinkle, Potential and limitations of ceramics in terms of structural and electrical integrity in fusion environments, J. Nucl. Mater. 233-237 (1996) 100-110.
[67] C.E. Kessel, The Fusion Nuclear Science Facility, the critical step in the pathway to fusion energy, Fusion Sci. Technol. 68(2) (2015).
[68] L. El-Guebaly, T. Huhn, A. Rowcliffe, S. Malang, A.-A. Team, Design challenges and activation concerns for ARIES vacuum vessel, Fusion Sci. Technol. 64(3) (2013) 449-454.
[69] R.L. Klueh, D.J. Alexander, P.J. Maziasz, Bainitic chromium-tungsten steels with 3 pct chromium, Metall. Mater. Trans. A-Phys. Metall. Mater. Sci. 28(2) (1997) 335-345.
[70] R.L. Klueh, E.T. Cheng, M.L. Grossbeck, E.E. Bloom, Impurity effects on reduced-activation ferritic steels developed for fusion applications, J. Nucl. Mater. 280(3) (2000) 353-359.
[71] M.T. Elias, L. El-Guebaly, Shielding and activation analyses for outboard region of FESS-FNSF design, University of Wisconsin-Madison, UWFDM-1424, (2015).
[72] B.M. Madani, L. El-Guebaly, Shielding and activation analyses for inboard region of FESS-FNSF design, University of Wisconsin-Madison, UWFDM-1423, (2015).

[73] K. Farrell, T.S. Byun, Tensile properties of ferritic/martensitic steels irradiated in HFIR and comparison with spallation neutron irradiation data, J. Nucl. Mater. 318 (2003) 274-282.
[74] R.L. Klueh, Elevated-temperature ferritic and martensitic steels and their application to future nuclear reactors, ORNL/TM-2004/176, (2004).
[75] R.L. Klueh, N.D. Evans, P. Maziasz, V.K. Sikka, Creep-rupture behavior of 3Cr-3W-V bainitic steels, Int. J. Pressure Vessels Pip. 84(1-2) (2007) 29-36.
[76] M. Jawad, V.K. Sikka, Development of a new class of Fe-3Cr-W(V) ferritic steels for industrial process applications, ORNL, ORNL/TM-2005/82, (2005).
[77] R.L. Klueh, A.M. Nasreldin, Microstructure and mechanical properties of a 3Cr-1.5Mo steel, Metallurgical Transactions A 18(7) (1987) 1279-1290.
[78] Y. Yamamoto, P.J. Maziasz, A.F. Rowcliffe, L.L. Snead, Development of advanced 3Cr-3WV(Ta) bainitic steels for fusion structural applications. Presented at ICFRM-17, October 12-16, 2015